ACS OMEGA

Open Access

http://pubs.acs.org/journal/acsodf

Article

Study on the Performance of Ni−MoS_2 Catalysts with Different MoS_2 Structures for Dibenzothiophene Hydrodesulfurization

Chuangchuang Yang, Anpeng Hu, Qiaoling Dai, Qinghe Yang,* Ranran Hou, and Zhiwei Liu

Cite This: *ACS Omega* 2023, 8, 41182−41193

Read Online

ACCESS | Metrics & More | Article Recommendations | Supporting Information

ABSTRACT: Hydrodesulfurization (HDS) is an important process for the production of clean fuel oil, and the development of a new environmentally friendly, low-cost sulfided catalyst is key research in hydrogenation technology. Herein, commercial bulk MoS_2 and $NiCO_3{\cdot}2NiOH_2{\cdot}4H_2O$ were first hydrothermally treated and then calcined in a H_2 or N_2 atmosphere to obtain Ni−MoS_2 HDS catalysts with different structures. Mechanisms of hydrothermal treatment and calcination on Ni−MoS_2 catalyst structures were investigated by X-ray diffraction (XRD), high-resolution transmission electron microscopy (HRTEM), electron paramagnetic resonance (EPR), and X-ray photoelectron spectroscopy (XPS). The catalytic performance of Ni−MoS_2 catalysts was evaluated by the HDS reaction of dibenzothiophene (DBT) on a fixed bed reactor, and the structure−activity relationship between the structures of the Ni−MoS_2 catalyst and the HDS of DBT was discussed. The results showed that the lateral size, the number of stacked layers, and the S/Mo atomic ratio of MoS_2 in the catalyst decreased and then increased with the increase of the hydrothermal treatment temperature, reaching the minimum at the hydrothermal treatment temperature of 150 °C, i.e., the lateral size of MoS_2 in the catalyst was 20−36 nm, the number of stacked layers of MoS_2 was 5.4, and the S/Mo ratio in the catalyst was 1.80. In addition, the effects of different calcination temperatures and calcination atmospheres on the catalyst structures were investigated at the optimum hydrothermal treatment temperature. The Ni−Mo−S and Ni_xS_y ratios of the catalysts increased and then decreased with the increasing calcination temperature under a H_2 atmosphere, reaching a maximum at a calcination temperature of 400 °C. Therefore, DBT exhibited the best HDS activity over the H-NiMo-150−400 catalyst, and the desulfurization rate of DBT reached 94.7% at a reaction temperature of 320 °C.

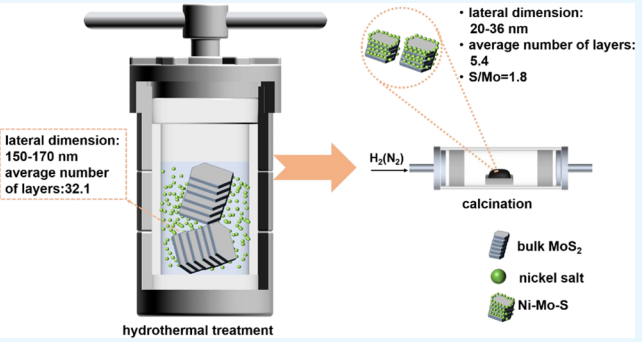

1. INTRODUCTION

In recent years, the production of clean fuels has faced serious challenges due to the substandard quality of crude oil, as well as the emphasis on environmental protection and increasingly stringent environmental regulations.[1,2] Hydrodesulfurization (HDS) is the main method to remove the heteroatoms in petroleum fractions and to produce clean fuels.[3] Because the catalyst is the core of HDS technology, the research on the HDS catalyst has attracted much attention.[4,5]

The most general and important hydrotreating catalysts, alumina or modified alumina-supported MoS_2 usually promoted by Co or Ni atoms, have been used in the refining industry for more than half a century.[6,7] In the industrial preparation of Mo-based hydrotreatment catalysts, solutions containing Ni^{2+} and oxidized molybdenum-containing anions, such as $Mo_7O_{24}^{6-}$ and $P_2Mo_5O_{23}^{6-}$, are usually first impregnated onto an Al_2O_3 support and then calcined to obtain an oxidized catalyst.[8,9] In refinery hydrogenation reactors, the oxidized catalysts are reduced to sulfides using a mixture of a feed of H_2 and of sulfur-containing compounds, such as H_2S, CS_2, dimethylsulfide (DMS), and dimethyldisulfide (DMDS).[10−12] In general, the strong interaction between the active metal and the Al_2O_3 support during calcination of the supported catalyst promotes the formation of the Mo−O−Al phase.[13] This strong interaction is conducive to the dispersion of Mo species to ensure high accessibility of the active sites to the reactants, but resulting in the subsequent sulfurization process needs to be carried out in a more stringent condition.[1,14] Furthermore, the formation of spinel phases between Co/Ni and Al_2O_3 adversely affects MoS_2 edge site catalytic performance.[15] In order to avoid the negative impact of the support on the catalyst, researchers[16,17] have proposed the preparation of unsupported HDS catalysts, which have been widely studied and become a new research direction due to their outstanding advantages, such as high utilization of active metals, high activity, and good resistance to carbon

Received: June 8, 2023
Revised: October 6, 2023
Accepted: October 11, 2023
Published: October 30, 2023

deposition. Liu et al.[17] first synthesized NiMo oxides by the poly(vinylpyrrolidone) (PVP)-assisted chemical precipitation method and then prepared highly active unsupported HDS catalysts by in situ sulfidation of CS_2 and H_2 mixture. Chowdari et al.[18] investigated the preparation of Ni−MoS_2 nanotubes from bulk NiMo oxides by different sulfidation methods. The results showed that the activity of the unsupported HDS catalyst prepared by in situ sulfidation was 4 times higher than that of the catalyst prepared by non-in-situ sulfidation. Afanasiev[19] prepared the unsupported Ni−MoS_2 catalysts by first decomposing ammonium tetrathiomolybdate (ATM) to MoS_2 at different temperatures and gas compositions and then introducing a promoter into the synthesized MoS_2 by dissolving the organic complex of nickel or cobalt in an organic solution for reflux.

Therefore, most supported and unsupported HDS catalysts are first oxidized and then sulfided with sulfur-containing compounds. The use of sulfur-containing compounds, which are usually highly toxic, not only poses serious environmental problems but also causes severe corrosion of equipment and pipelines. In addition, the sulfidation process prolongs the refinery's startup time, which is detrimental to the economics of the refinery.[20−22] The preparation of sulfurized catalysts by simultaneous decomposition of precursors containing S and Mo, such as ATM, has the disadvantages of a complex precursor preparation process and a high price and is not suitable for industrial applications. To solve these problems, researchers are looking for an environmentally friendly and inexpensive precursor containing S and Mo. Researchers[23,24] proposed to prepare HDS catalysts using MoS_2, which is the active component of HDS catalysts and can be obtained by direct purification from molybdenum pyroxene concentrates.[25,26] Based on the rim-edge model for unloaded HDS catalysts,[27,28] the active sites responsible for the HDS reaction are situated at the rim sites located at the top and bottom of the layer-stacked MoS_2, as well as the edge sites positioned between these upper and lower regions. Conversely, the basal surface of MoS_2 remains inert. However, when MoS_2 is obtained from molybdenum pyroxene concentrates, it exhibits a substantial transverse size of lamellar crystals (>150 nm) and a significant number of stacked layers (>30 layers). Consequently, this configuration exposes fewer rim and edge sites, thereby restricting the HDS activity. Wang et al.[2] obtained MoS_2 with a lateral size of about 30 nm and a stacking number of 6−8 layers by ball milling multilayers of commercial MoS_2 with large lateral sizes. They found that ball milling exposed more Rim active sites of MoS_2, thus improving the hydrogenation activity of the catalyst. Mahmoudabadi et al.[23] prepared MoS_2/GO catalysts by ultrasonic coexfoliation of commercial bulk MoS_2 and graphene (GO) assisted by poly(vinylpyrrolidone) (PVP). The results showed that the HDS activity of MoS_2/GO was higher than that of the conventional loaded catalysts. The promoter Ni/Co can exponentially increase the activity of the catalyst by modifying the MoS_2 edge and increasing the electron cloud density of the adjacent Mo atoms. However, to the best of our knowledge, there are fewer studies focusing on the effects of Ni/Co atoms on the HDS catalysts prepared by modifying commercial MoS_2, and furthermore, the different structures of MoS_2 and the performance of HDS catalysts need to be further investigated.

Here, commercial bulk MoS_2 and $NiCO_3{\cdot}2NiOH_2{\cdot}4H_2O$ were first hydrothermally treated and then calcined in a H_2 or N_2 atmosphere to obtain Ni−MoS_2 hydrodesulfurization catalysts with different structures. The mechanisms of hydrothermal treatment and calcination on the structure of the Ni−MoS_2 catalyst were investigated by X-ray diffraction (XRD), high-resolution transmission electron microscopy (HRTEM), electron paramagnetic resonance (EPR), and X-ray photoelectron spectroscopy (XPS). The HDS performance of the Ni−MoS_2 catalyst was evaluated in a fixed bed reactor using DBT as a model compound, and the structure−activity relationship between the structure of the Ni−MoS_2 catalyst and the HDS of DBT was discussed.

2. EXPERIMENTAL SECTION

2.1. Materials. No further purification was performed on all of the materials once they were received. Commercial bulk molybdenum disulfide (MoS_2) was purchased from Aladdin Industrial Co. Basic nickel carbonate ($NiCO_3{\cdot}2Ni(OH)_2{\cdot}4H_2O$) was supplied by the SINOPEC Changling Catalyst Company. Dibenzothiophene (DBT) and decalin were supplied by J&K Chemical, and *n*-decane was purchased from Tianjin Damao Chemical Reagent Factory.

2.2. Preparation of Sulfided NiMo Catalysts. A series of sulfided NiMo HDS catalysts were prepared by hydrothermal treatment of commercial bulk molybdenum disulfide (b-MoS_2) and basic nickel carbonate ($NiCO_3{\cdot}2Ni(OH)_2{\cdot}4H_2O$), according to the Ni/Mo atomic ratio of 0.5 at a certain temperature, and then calcined under a nonoxidizing atmosphere. Typically, 5 g of commercial MoS_2 powder, 1.96 g of $NiCO_3{\cdot}2Ni(OH)_2{\cdot}4H_2O$ powder, and 70 mL of deionized water were added to a 100 mL Teflon-lined stainless steel rotary autoclave and hydrothermally treated at 90, 120, 150, 180, and 200 °C for 10 h, respectively. The black precipitate acquired through filtration is subjected to washing with deionized water, subsequent air drying at a temperature of 120 °C for a duration of 6 h, and subsequently undergoing calcination in a H_2 atmosphere at temperatures of 350, 400, 500, and 600 °C for a duration of 3 h. Additionally, the mixture is calcined in a N_2 atmosphere at a temperature of 400 °C for a duration of 3 h. The prepared catalysts were named H-NiMo-*x*-*y* and N-NiMo-*x*-*y*, where *x* represents the hydrothermal treatment temperature and *y* represents the calcination temperature.

Furthermore, to examine the impact of hydrothermal treatment and calcination in a hydrogen atmosphere on the structure of the catalyst, two separate catalysts were prepared: the NiMo-150 catalyst solely subjected to hydrothermal treatment without calcination and the H-NiMo-400 catalyst solely subjected to calcination in a hydrogen atmosphere without hydrothermal treatment. In this experiment, a 100 mL Teflon-lined stainless steel rotary autoclave was utilized to combine 5 g of commercial MoS_2 powder, 1.96 g of $NiCO_3{\cdot}2Ni(OH)_2{\cdot}4H_2O$ powder, and 70 mL of deionized water. The resulting mixture was subjected to hydrothermal treatment at a temperature of 150 °C for a duration of 10 h. The resulting black precipitate was then filtered and washed with deionized water before being dried at 120 °C for 6 h, resulting in the formation of NiMo-150. In a separate procedure, the same quantities of MoS_2, $NiCO_3{\cdot}2Ni(OH)_2{\cdot}4H_2O$, and deionized water were combined in a beaker, and the mixture was stirred for 10 h at room temperature. The resulting black precipitate was filtered, washed with deionized water, and subsequently dried at 120 °C for 6 h. This dried precipitate was then subjected to calcination in a H_2 atmosphere at a temperature of

https://doi.org/10.1021/acsomega.3c04059
ACS Omega 2023, 8, 41182−41193

Scheme 1. HDS Reaction Pathways of DBT

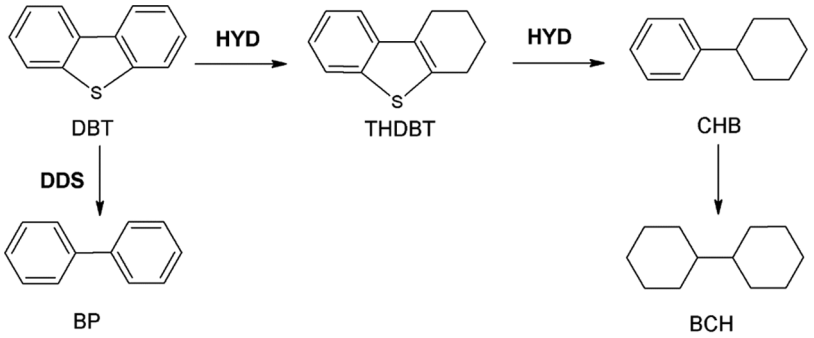

400 °C for a duration of 3 h, resulting in the formation of H-NiMo-400.

2.3. Characterization of Catalysts. The X-ray diffraction measurements were carried out on a Bruker D5005 X′ Pert diffractometer with Cu Kα radiation (λ = 1.5406 Å). Patterns were collected from 5 to 70° at a scanning speed of 2° min^{-1}. The Bragg equation ($d = n\lambda/2 \sin\theta$) was used to calculate the interlayer spacing of the (002) crystal plane of MoS_2. High-resolution transmission electron microscopy (HRTEM) was performed on a Philips Tecnai G2 F20 instrument with an electron energy of 200 kV, a conductive concentration of 0.5 mm, a resolution of 1.9 Å in TEM mode, and a sample tilt of ±40°. Images were captured with a TVIPS 1k × 1k CCD camera. In order to obtain an objective assessment of the lateral dimensions and stacking layers of MoS_2 samples, we conducted a random count of 50 MoS_2 nanosheets from the HRTEM images for each MoS_2 sample. Subsequently, we computed the lateral dimension and average number of stacking layers. The X-ray photoelectron spectroscopy (XPS) studies were performed using an ESCALab250 spectrometer from VG Scientific. Element surface area was quantified using the sensitivity factors provided by the VG program. All binding energies (BEs) were calibrated to C 1s, a form of adventitious carbon (284.80 eV). In addition, Avantage software (version 5.967) can be used to fit the XPS spectrum to identify the chemical states of the Ni species (namely, Ni−Mo−S, Ni^{2+}, Ni_xS_y, Ni shakeup). The Bruker A330 X-band continuous wave EPR spectrometer was utilized to measure the electron paramagnetic resonance (EPR) spectra. The paramagnetic samples were positioned within a rectangular resonator operating at a frequency of 9.853301 GHz. The surface morphology and the composition of the samples were characterized using scanning electron microscopy (SEM, JEOL JSM-6700F) and energy dispersive spectroscopy (EDS, Hitachi S-4800-I).

2.4. Catalytic Performance of Catalysts. The catalytic activities of sulfided NiMo catalysts were evaluated in a 500 mm long, 10.0 mm diameter fixed microreactor. The catalyst was ground to 40−60 mesh, and 0.45 g of catalyst was diluted with 1 g of quartz sand; then, the diluted sample was added to the constant temperature zone of the reactor, and the remainder was filled with 40−60 mesh quartz sand. A 1 wt % dibenzothiophene (DBT)/*n*-decane solution was chosen as the model reactant. HDS reactions of DBT were conducted at 260, 280, 300, and 320 °C, total pressure 4 MPa, WHSV 24.67 h^{-1}, and H_2/feed volume ratio of 500. The hydrodesulfurization products were analyzed on an Agilent 7890A series gas chromatograph, and decalin was used as an internal standard to calculate the content of each component in the product by normalization. According to the equation below, the conversion (denoted as x) of the reaction can be calculated.

$$x = \left(1 - \frac{\mathrm{DBT}_{\text{after reaction}}}{\mathrm{DBT}_{\text{intial}}}\right) \times 100\%$$

The HDS reaction of DBT occurs via two primary pathways, specifically hydrogenation (HYD) and direct desulfurization (DDS), as depicted in Scheme 1.[29−31] In the DDS pathway, DBT completes the reaction by directly breaking the C−S bond at the S vacancy of the catalyst through the S atom adsorbed in the σ mode to form biphenyl (BP); in the HYD pathway, DBT is adsorbed onto the catalyst in the π-mode via the aromatic system and is first hydrogenated to form the intermediate tetrahydrodibenzothiophene (THDBT), which is then desulfided to form cyclohexylbenzene (CHB) and bicyclohexane (BCH).[29,32] As a result of gas chromatography-mass spectrometry (GC-MS) analysis, several products were detected in the HDS of DBT. As hydrogenated intermediates in the hydrogenation (HYD) pathway, tetrahydrodibenzothiophene (THDBT) is further desulfurized to form cyclohexylbenzene (CHB) and bicyclohexane (BCH), and direct desulfurization (DDS) produces biphenyl (BP). The following equations were used to calculate the selectivity

$$S_{\mathrm{DDS}} = \frac{[\mathrm{BP}]}{[\mathrm{THDBT}] + [\mathrm{BP}] + [\mathrm{CHB}] + [\mathrm{BCH}]} \times 100\%$$

$$S_{\mathrm{HYD}} = \frac{[\mathrm{THDBT}] + [\mathrm{CHB}] + [\mathrm{BCH}]}{[\mathrm{THDBT}] + [\mathrm{BP}] + [\mathrm{CHB}] + [\mathrm{BCH}]} \times 100\%$$

3. RESULTS AND DISCUSSION

3.1. Effect of Hydrothermal Treatment Temperature on the Structure of Sulfided NiMo Catalysts. *3.1.1. XRD Analysis.* Figure 1 shows the XRD patterns of b-MoS_2 and sulfided NiMo catalysts prepared at different hydrothermal treatment temperatures. It can be seen from Figure 1 that the diffraction peaks are at 14.4, 32.7, 33.5, 58.4°, etc., in the XRD pattern of b-MoS_2 corresponding to planes (002), (100), (101), (110), etc., in hexagonal 2H-MoS_2 (JCPDS No. 37−1492). Compared with that of b-MoS_2, the characteristic peak intensity of each crystal plane of sulfided NiMo prepared by different hydrothermal treatment temperatures is obviously reduced. Especially, the intensity of the (002), (100), and (110) characteristic peaks is reduced for the (002) crystal plane, representing the number of MoS_2 stacking layers, and the (100) crystal plane and (110) crystal plane, representing the lateral size of MoS_2, which means the reduction of the stacking layers and lateral size of the prepared catalysts.[2,33] In

https://doi.org/10.1021/acsomega.3c04059
ACS Omega 2023, 8, 41182−41193

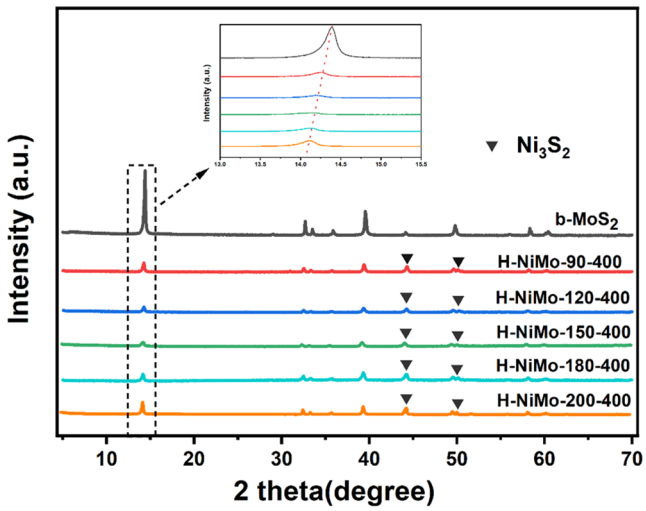

Figure 1. XRD patterns of sulfided NiMo catalysts obtained at different hydrothermal treatment temperatures.

the high-temperature and high-pressure hydrothermal environment, a large amount of high-pressure airflow accelerates the MoS_2 extension and distortion, thus leading to a certain degree of disruption of the van der Waals forces between MoS_2 layers and Mo−S bonds within the layers.[34,35] At the same time, due to the adsorption of Ni salt on the surface of MoS_2,[36−38] the reaggregation of exfoliated MoS_2 is prevented. When the hydrothermal temperature was increased from 90 to 150 °C, the intensity of the diffraction peaks, especially the (002) peak in the XRD patterns of the obtained catalyst samples, first gradually decreased and then showed a gradual increase as the hydrothermal temperature continued to increase from 150 to 200 °C. This may be due to the partial desorption of $NiCO_3 \cdot 2Ni(OH)_2 \cdot 4H_2O$ adsorbed on the MoS_2 surface, resulting in slight aggregation of MoS_2 as the hydrothermal treatment temperature continues to increase.[37,39]

Interestingly, as shown in the amplified spectrum in Figure 1, the characteristic peak of the (002) crystal plane of the resulted catalyst is slightly shifted to a lower angle than that of b-MoS_2, indicating a slight expansion of the MoS_2 interlayer spacing caused by the lattice distortion of the catalyst.[40] The results of calculations based on the Bragg equation (Table 1) show that the interlayer spacing of MoS_2 increases with an increase in the hydrothermal treatment temperature. Increasing the MoS_2 layer spacing could potentially facilitate the adsorption and desorption of reactant molecules (DBT) on the active sites, thereby contributing to the enhancement of the HDS activity.[41,42]

Table 1. Interlayer Spacing, Lateral Dimensions, and Number of Stacked Layers of Commercially Available Molybdenum Disulfide and Sulfided NiMo Catalysts with Different Hydrothermal Treatments

catalysts	2θ (deg)	interlayer spacing (Å)	lateral dimension (nm)	average number of layers
b-MoS_2	14.41	6.14	150−170	32.1
H-NiMo-90−400	14.27	6.20	45−55	6.6
H-NiMo-120−400	14.23	6.22	35−47	6.2
H-NiMo-150−400	14.19	6.24	20−36	5.4
H-NiMo-180−400	14.16	6.25	37−50	6.8
H-NiMo-200−400	14.13	6.26	47−60	7.1

Furthermore, the diffraction peaks at $2\theta = 44.3$ and 50.1° in the XRD spectra of sulfided NiMo catalysts can be indexed to the (202) and (211) crystal planes of Ni_3S_2, which is in good agreement with the standard Ni_3S_2 (JCPDS card number 44−1418) and previous studies.[43−45]

3.1.2. HRTEM Analysis. The morphology and microstructure of sulfided NiMo catalysts obtained from different hydrothermal treatment temperatures were studied with high-resolution TEM (HRTEM). As shown in Figure 2, the stripes with a lattice spacing of about 0.62 nm correspond to the (002) plane of hexagonal MoS_2. The commercial bulk molybdenum disulfide (b-MoS_2) sample is composed of regular sheets with lateral sizes of several hundred nanometers and stacked layers of more than 30 (Figure 2a), while the lateral size and stacked layers of MoS_2 in the catalyst samples prepared by hydrothermal treatment are significantly reduced, which is consistent with the XRD results. In addition, the large number of discontinuous lattice stripes found in the hydrothermally treated catalysts indicated the presence of abundant structural defects[46,47] (Figure 2b,c,d,e,f). The reduction of MoS_2 lateral size and stacking layer number as well as the presence of defects would favor the catalyst to expose more active sites and thus increase the HDS activity.[2,48] The statistics of lateral dimensions and the average number of stacked layers of MoS_2 for HRTEM images are shown in Table 1. As can be seen in Table 1, when the hydrothermal treatment temperature was increased from 90 to 150 °C, the lateral size and the number of stacked layers of MoS_2 in the obtained catalysts first gradually decreased and then rather slightly increased with further increasing the hydrothermal treatment temperature, which is consistent with the XRD results.

3.1.3. EPR and SEM-EDS Analyses. To conduct a more thorough investigation into the S vacancies of the catalysts synthesized at various hydrothermal temperatures, the catalysts underwent EPR characterization. The EPR spectra of the catalysts prepared with b-MoS_2 at different hydrothermal temperatures are depicted in Figure 3. The spectra reveal that all samples exhibit the lowest EPR signal at $g = 0.2003$. The intensity of the EPR signal directly correlates with the concentration of S vacancies,[49−51] and the peak intensity of the prepared catalysts surpasses that of b-MoS_2. This observation implies that the catalysts possess a higher abundance of sulfur vacancies. The sulfur vacancy concentration of the catalysts prepared at different hydrothermal temperatures decreases in the following order: H-NiMo-150−400 > H-NiMo-120−400 > H-NiMo-180−400 > H-NiMo-90−400 > H-NiMo-200−400. Figure S6 displays the typical SEM micrographs and EDS spectra of H-NiMo-150−400, revealing a uniform dispersion of Ni in the catalyst. Table 2 presents the elemental contents and S/Mo atomic ratios of b-MoS_2 and the catalysts prepared at various hydrothermal treatment temperatures, as determined by EDS analysis. The catalysts exhibit varying concentrations of S vacancies, with a decreasing trend observed in the following sequence: H-NiMo-150−400 > H-NiMo-120−400 > H-NiMo-180−400 > H-NiMo-90−400 > H-NiMo-200−400.

3.1.4. XPS Analysis. The chemical composition and valence states in the sulfided NiMo catalysts obtained at different hydrothermal treatment temperatures were further investigated by XPS, and the Mo 3d and S 2p spectra of the six samples are shown in Figure 4. Spectra were fitted by Gaussian−Lorentzian

https://doi.org/10.1021/acsomega.3c04059
ACS Omega 2023, 8, 41182−41193

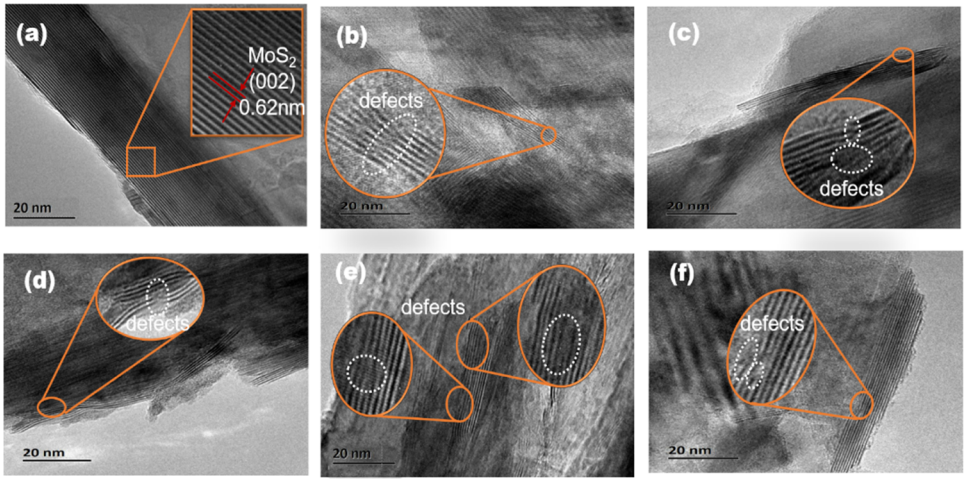

Figure 2. HRTEM images of sulfided NiMo catalysts obtained at different hydrothermal treatment temperatures: (a) b-MoS_2, (b) H-NiMo-90−400, (c) H-NiMo-120−400, (d) H-NiMo-150−400, (e) H-NiMo-180−400, and (f) H-NiMo-200−400.

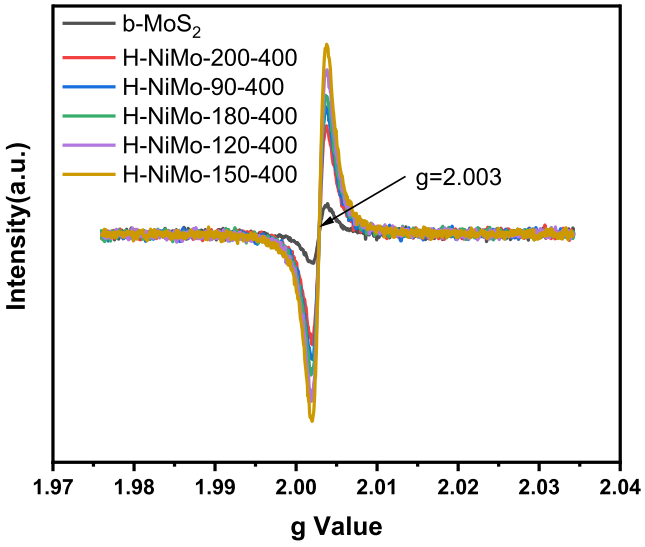

Figure 3. EPR patterns of sulfided NiMo catalysts obtained at different hydrothermal treatment temperatures.

curves, and the peak shifts were corrected by using the standard C 1s peak at 284.6 eV.[2,40] As shown in Figure 4a, the binding energies are located at about 229.0 and 232.1 eV attributed to the Mo $3d_{5/2}$ and Mo $3d_{3/2}$ characteristic peaks of Mo^{4+}, while the binding energies of Mo^{6+} appear at about 232.5 and 235.7 eV, and the binding energy of the S 2s peak appears at about 226.2 eV.[1,52] In the S 2p fitting spectrum illustrated in Figure 4b, the observed peaks at 162.3 and 163.5 eV in the b-MoS_2 sample can be ascribed to the S $2p_{3/2}$ and S $2p_{1/2}$ orbitals of S^{2-}, respectively. The peak at 169.6 eV is a characteristic peak due to the partial oxidation of S on the MoS_2 surface to form SO_4^{2-}.[53,54] Interestingly, the Mo 3d peaks of the catalyst samples prepared by hydrothermal treatment were shifted by about 0.3 eV toward lower binding energies compared to commercial bulk molybdenum disulfide (b-MoS_2), while the same shift occurred for S 2p peaks. The lower binding energy of the Mo 3d signal and the S 2p signal of the catalysts (Ni_3S_2−MoS_2) prepared by hydrothermal treatment indicates not only a strong electronic interaction between Ni_3S_2 and MoS_2 in the catalysts[55,56] but also a reduction in the number of S atoms and the creation of S vacancies,[57,58] which contributes to the HDS reactivity of the catalysts.[59,60] Table 3 shows the S/Mo atomic ratios of the six samples based on the XPS peak area ratio between S 2p and Mo 3d. It can be seen from Table 3 that the S/Mo atomic ratio in the sulfided NiMo catalyst is lower compared to that of b-MoS_2, further confirming the presence of a large number of S vacancies in the catalyst samples prepared by hydrothermal treatment. The number of S vacancies in the catalyst decreases in the following order: H-NiMo-150−400 > H-NiMo-120−400 > H-NiMo-180−400 > H-NiMo-90−400 > H-NiMo-200−400, which is consistent with the results of EPR and SEM-EDS.

The Ni $2p_{3/2}$ spectra and corresponding deconvolution curves of sulfided NiMo catalysts at different hydrothermal treatment temperatures are shown in Figure 5. There is about 854.1 eV binding energy for the Ni $2p_{3/2}$ peak for the Ni−Mo−S active phase, 853.2 eV for Ni_xS_y, and 856.7 eV for oxidized Ni^{2+} species.[1,61] The peaks observed at an energy level of 862.2 eV are attributed to the shakeup satellite structures originating from the Ni $2p_{3/2}$ orbital.[1] Many studies concluded that Ni_xS_y in the catalyst is less active in the HDS reaction,[62−64] but the presence of a certain amount of Ni_xS_y

Table 2. EDS Results of Catalysts Prepared at Different Hydrothermal Treatment Temperatures

catalysts	Ni, %	Mo, %	S, %	O, %	Ni/Mo	S/Mo
b-MoS_2	0	32.12	63.62	4.26	0	1.98
H-NiMo-90−400	12.02	28.35	54.19	5.44	0.42	1.91
H-NiMo-120−400	12.95	27.42	51.66	7.97	0.47	1.88
H-NiMo-150−400	14.96	26.79	49.22	9.03	0.56	1.84
H-NiMo-180−400	11.22	28.29	53.48	7.01	0.4	1.89
H-NiMo-200−400	14.27	27.63	53.17	4.93	0.52	1.92

https://doi.org/10.1021/acsomega.3c04059
ACS Omega 2023, 8, 41182−41193

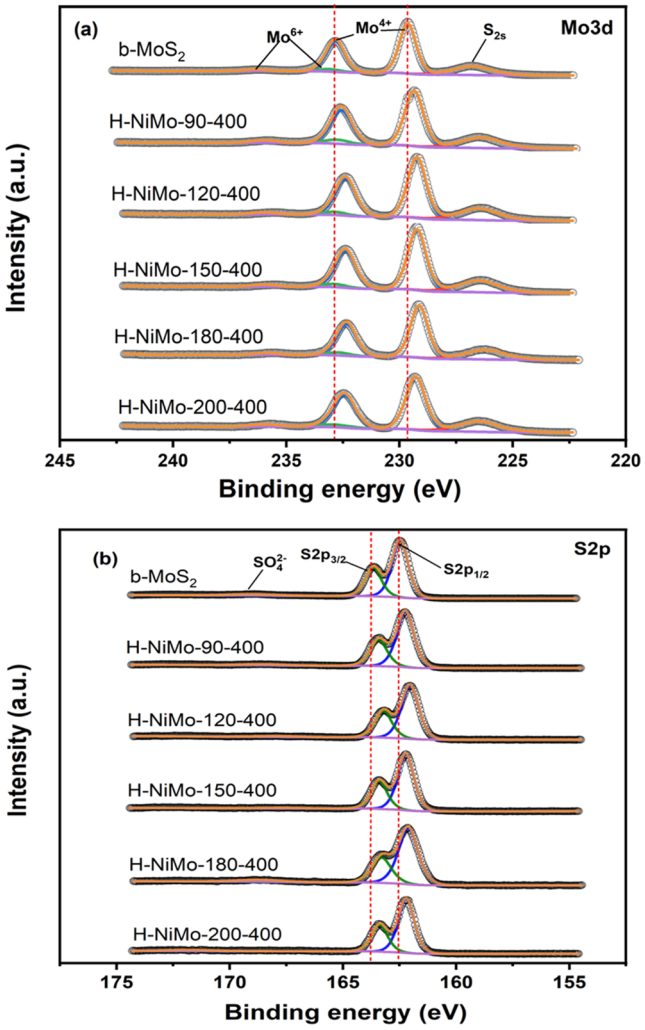

Figure 4. Fitted curves corresponding to Mo 3d and S 2p for sulfided NiMo catalysts obtained at different hydrothermal treatment temperatures: (a) Mo 3d fitted spectrum and (b) S 2p fitted spectrum.

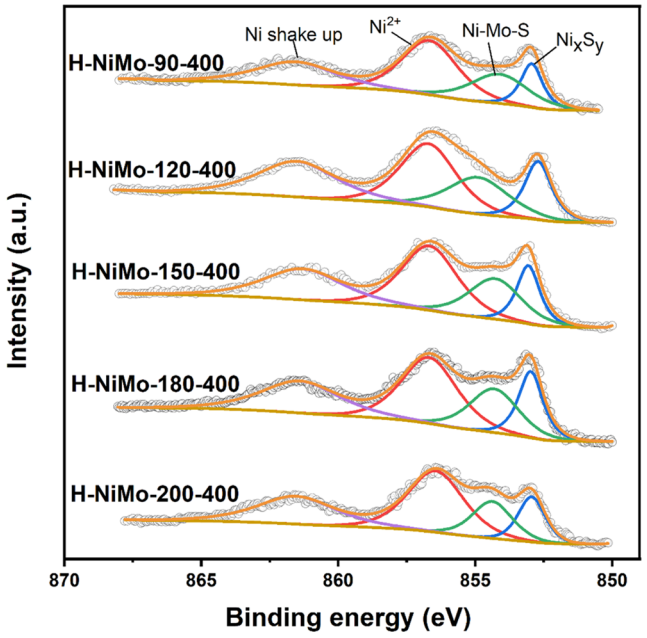

Figure 5. Ni $2p_{3/2}$ spectra and corresponding deconvoluted curves of sulfided NiMo catalysts obtained at different hydrothermal treatment temperatures.

can take a synergistic effect with MoS_2, making the hydrogen spillover effect more effective and thus improving the HYD selectivity of DBT.[59,65−68] The proportion of active species at different hydrothermal treatment temperatures is shown in Table 3. The relative proportions of active species (Ni−Mo−S + Ni_xS_y) decrease in the following order: H-NiMo-150−400 > H-NiMo-120−400 > H-NiMo-180−400 > H-NiMo-90−400 > H-NiMo-200−400.

3.2. Effects of Different Calcination Conditions (Temperature and Atmosphere) on the Structure of Sulfided NiMo Catalysts. *3.2.1. XRD Analysis.* Calcination is a key process for $NiCO_3{\cdot}2Ni(OH)_2{\cdot}4H_2O$ to decompose and interact with MoS_2 to form Ni−Mo−S and Ni_xS_y. The optimum hydrothermal treatment temperature was selected to study the effects of different calcination temperatures and calcination atmospheres on the catalyst structure. The XRD patterns of the sulfided NiMo catalysts with different calcination temperatures and calcination atmospheres are shown in Figure 6. The XRD spectra of the H-NiMo-150−350 sample calcinated at 350 °C in a H_2 atmosphere showed only the characteristic peaks of MoS_2, but the characteristic peaks of Ni_3S_2 appeared at 2θ = 44.4 and 50.2° for H-NiMo-150−400. The presence of Ni_3S_2 in the H-NiMo-150−400 sample was able to prevent the aggregation of MoS_2, and then, the intensity of the MoS_2 characteristic peak was reduced. The spectra of H-NiMo-150−500 and H-NiMo-150−600 exhibit a greater number of Ni_3S_2 peaks at 2θ = 21.8, 31.1, 37.8, 54.6, and 55.3°, along with a continuous increase in the intensities of these characteristic peaks from a calcination temperature of 400 to 600 °C. This phenomenon can be attributed to the reduction in edge sites caused by the sintering of MoS_2 at higher calcination temperatures. Consequently, the availability of Ni for accommodation at the MoS_2 edge to form the Ni−Mo−S phase decreases, leading to the generation of thermodynamically stabilized Ni_3S_2 in a calcined environment. This finding aligns with previous research.[69−71] Moreover, the

Table 3. S/Mo Atomic Ratio and Different Ni Species Proportions of Commercial Molybdenum Disulfide and Sulfided NiMo Catalysts with Different Hydrothermal Treatments

catalysts	S/Mo	Ni^{2+}, %	Ni−Mo−S, %	Ni_xS_y, %	Ni−Mo−S + Ni_xS_y, %
b-MoS_2	2.02	0	0	0	0
H-NiMo-90−400	1.88	66.3	18.9	14.8	33.7
H-NiMo-120−400	1.83	62.7	21.0	16.3	37.3
H-NiMo-150−400	1.80	57.7	23.4	18.9	42.3
H-NiMo-180−400	1.84	63.7	20.8	15.5	36.3
H-NiMo-200−400	1.89	68.1	18.0	13.9	31.9

https://doi.org/10.1021/acsomega.3c04059
ACS Omega 2023, 8, 41182−41193

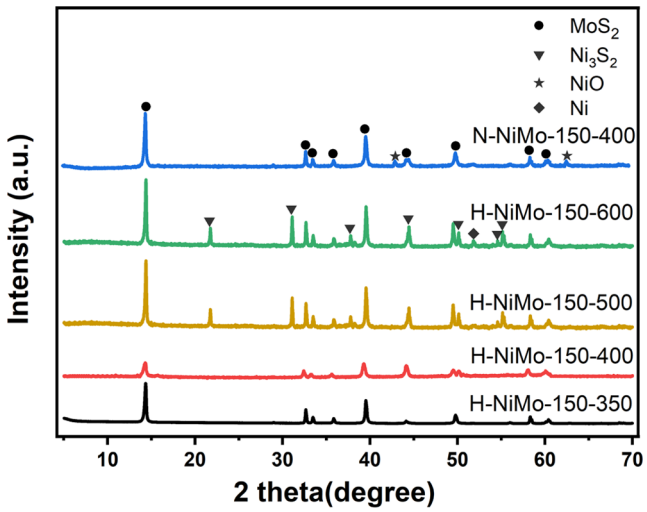

Figure 6. XRD patterns of sulfided NiMo catalysts obtained at different calcination temperatures and calcination atmospheres.

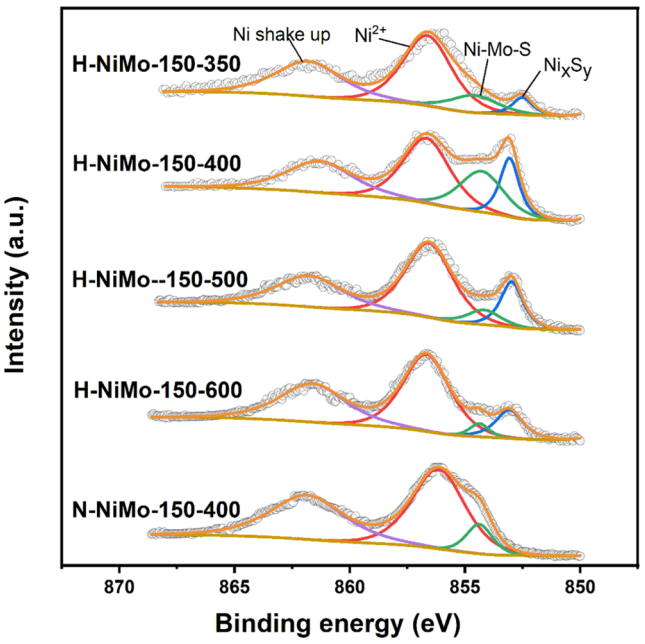

Figure 7. Ni $2p_{3/2}$ spectra and corresponding deconvoluted curves of sulfided NiMo catalysts obtained at different calcination temperatures and calcination atmospheres.

diffraction peak at $2\theta = 51.9°$ in the spectrum of the H-NiMo-150−600 sample was attributed to Ni (JCPDS No. 87−0712), which can be ascribed to the reduction of Ni species (NiO or Ni_xS_y) in the catalyst when the calcination temperature was increased to 600 °C in a H_2 atmosphere. Unlike the catalyst samples prepared by calcination in a H_2 atmosphere, the XRD spectra of the catalyst N-NiMo-150−400 samples prepared by calcination of the catalyst precursor at 400 °C in a N_2 atmosphere do not exhibit the diffraction peak of Ni_3S_2 but exhibit the characteristic peaks of NiO at $2\theta = 37.2$ and 62.8°. When the catalyst precursor was calcined in a N_2 atmosphere, $NiCO_3{\cdot}2Ni(OH)_2{\cdot}4H_2O$ adsorbed on the surface of MoS_2 decomposed into NiO.[72,73] At the same time, the decomposition of $NiCO_3{\cdot}2Ni(OH)_2{\cdot}4H_2O$ into NiO still exists during calcination in a H_2 atmosphere, but the process was also accompanied by the activation on some S in MoS_2 by H_2[74] and the activated S combined with Ni species to produce Ni_3S_2.

3.2.2. XPS Analysis. XPS was used to further characterize the chemical state of Ni species on the surface of the catalysts prepared at different calcination temperatures and calcination atmospheres, and the XPS fitted spectra of Ni species are shown in Figure 7. The active components Ni−Mo−S and Ni_xS_y of the catalysts calcined in a H_2 atmosphere were at 854.1 and 853.2 eV,[1,61] respectively, while the Ni $2p_{3/2}$ fitted spectra of the catalyst N-NiMo-150−400 calcined in a N_2 atmosphere contained only a small fraction of the Ni−Mo−S peaks. The proportions of different Ni species for the catalysts with different calcination temperatures and calcination atmospheres are shown in Table 4. As can be seen in Table 4, the percentages of active catalyst components (Ni−Mo−S and Ni_xS_y) obtained by calcination in a H_2 atmosphere showed a trend of increasing and then decreasing with the increased calcination temperature, reaching a maximum at a calcination temperature of 400 °C. According to the widely accepted Ni−Mo−S model,[75,76] Ni replaces some of Mo at the edges of MoS_2. When the calcination temperature is 350 °C, the incomplete decomposition of Ni salts and the limited activation reaction of H_2 on S in MoS_2 limits the Ni substitution of Mo at the edges of MoS_2 so that the Ni−Mo−S and Ni_xS_y percentages in the H-NiMo-150−350 sample are smaller than those in the H-NiMo-150−400 sample. With the progressive increase in calcination temperature under a H_2 atmosphere, the sintering of MoS_2 intensifies, resulting in a reduction of its edge sites that can accommodate Ni and facilitate the formation of Ni−Mo−S. Additionally, the elevated temperature leads to the segregation of Ni species from MoS_2, further generating Ni_3S_2.[69−71] Consequently, the Ni_xS_y/Ni−Mo−S ratios increase as the calcination temperature increases. When the catalyst precursor was calcined in a N_2 atmosphere, the Ni salt adsorbed on the MoS_2 surface interacted with MoS_2 during decomposition, causing Ni to partially replace Mo at the edge of MoS_2 to form a Ni−Mo−S structure. The irreducible N_2 could not activate the S in MoS_2 to react with the decomposed Ni salt to form Ni_xS_y, so only a small amount of Ni−Mo−S was formed in the N-NiMo-150−400 sample.

Table 4. Percentage of Ni Species for Different Calcination Temperatures and Calcination Atmospheres

catalysts	Ni^{2+}, %	Ni−Mo−S, %	Ni_xS_y, %	Ni−Mo−S + Ni_xS_y, %
H-NiMo-150−350	77.3	14.7	8.0	22.7
H-NiMo-150−400	57.7	23.4	18.9	42.3
H-NiMo-150−500	78.0	8.4	13.6	22.0
H-NiMo-150−600	82.1	5.7	12.2	17.9
N-NiMo-150−400	90.9	9.1	0	9.1

3.3. Catalytic Activity and Selectivity. DBT was used as a reactant to evaluate the HDS catalytic performance of samples. The relationship between the conversion and reaction temperature of DBT for the reaction on different catalysts is shown in Figure 8. The conversion of DBT increased with an increase of the reaction temperature. The conversion of DBT over sulfided NiMo catalysts was much higher than that of the commercial bulk molybdenum disulfide (b-MoS_2) sample at the same reaction temperature, which was attributed to the addition of the promoter Ni that could change the electronic properties of the active center and form a new Ni−Mo−S active phase, thus improving the HDS catalytic activity.[29,32] In

https://doi.org/10.1021/acsomega.3c04059
ACS Omega 2023, 8, 41182−41193

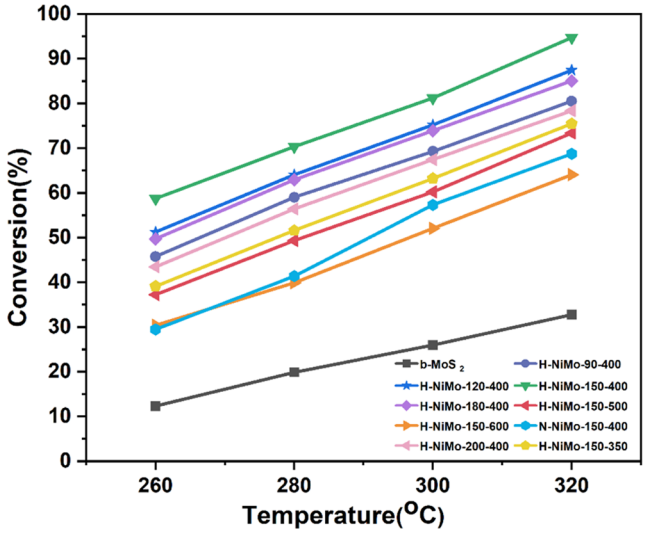

Figure 8. Temperature dependence of the DBT conversion on different catalyst samples.

addition, the conversion of DBT reacted on other catalysts except the catalyst N-NiMo-150−400 obtained by calcination in a N_2 atmosphere was almost linear with increasing temperature. According to the results of XRD (Figure 6) and XPS (Figure 7), the existing state of Ni species in the catalyst N-NiMo-150−400 is mainly NiO, and DBT acts as a sulfiding agent to further sulfide NiO into Ni_xS_y and Ni−Mo−S active phases under reaction conditions, and the fitted spectrum of Ni $2p_{3/2}$ of the reacted N-NiMo-150−400 sample is shown in Figure 9. Therefore, the conversion of DBT in N-NiMo-150−400 was significantly increased at the reaction temperature of 300 °C.

The order of activity for the sulfided NiMo catalysts, which were subjected to calcination under a hydrogen atmosphere, can be observed in Figure 7. The ranking, from highest to lowest, is as follows: H-NiMo-150−400, H-NiMo-120−400, H-NiMo-180−400, H-NiMo-90−400, H-NiMo-200−400, H-NiMo-150−350, H-NiMo-150−500, and H-NiMo-150−600.

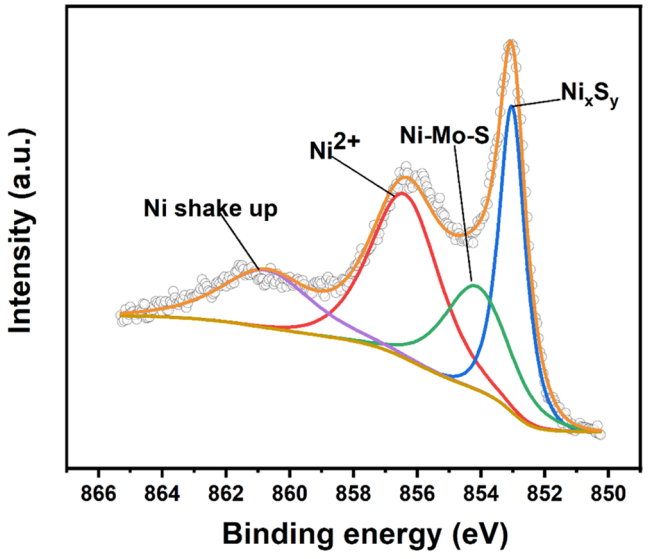

Figure 9. Ni $2p_{3/2}$ spectra and corresponding deconvoluted curves of N-NiMo-150−400 after the reaction.

The catalyst activity was found to be influenced by several key factors, including the quantity of active sites in MoS_2, the presence of sulfur vacancies, and the concentration of active components (Ni−Mo−S and Ni_xS_y) within the catalyst.[5,29,40] As the hydrothermal treatment temperature increases, the lateral size, the number of stacked layers, and S/Mo atomic ratio of MoS_2 in the catalyst first decrease and then increase (Tables 1, 2, and 3), reaching a minimum when the hydrothermal treatment temperature is 150 °C, i.e., in the following order: H-NiMo-150−400 < H-NiMo-120−400 < H-NiMo-180−400 < H-NiMo-90−400 < H-NiMo-200−400. The smaller lateral size of MoS_2 and the reduced number of stacked layers are more favorable for the exposed active sites.[2,77] Additionally, these factors promote the formation of a higher proportion of Ni−Mo−S and Ni_xS_y during the calcination process, thereby contributing to the improved activity of the catalyst.[78,79] At the same time, the smaller S/Mo ratio indicates the higher number of S vacancies in the catalyst,[80−82] which helps to improve the activity of the DBT reaction on the catalyst. Therefore, the order of activity of the DBT reaction on the catalyst is consistent with the results of XRD (Figure 1 and Table 1), TEM (Figure 2 and Table 1), ERP (Figure 3), SEM-EDS (Table 2), and XPS (Figure 4 and Table 3) characterization. Due to the incomplete decomposition of Ni salts[83,84] and the limited activation of H_2 and S in MoS_2,[32] the content of active components in the H-NiMo-150−350 sample was lower than that in H-NiMo-150−400 (Table 4), which made the conversion rate of DBT in H-NiMo-150−350 lower than that in H-NiMo-150−400. As the calcination temperature continued to increase, the Ni−Mo−S structure began to decompose continuously to form Ni_3S_2 and to detach from MoS_2,[78,85] which not only made the aggregation of MoS_2 and Ni_3S_2 increase (Figure 6) but also lead to the proportion of active components decrease (Table 4), resulting in lower conversion of DBT on the H-NiMo-150−500 and H-NiMo-150−600 samples than on the H-NiMo-150−400 sample.

The selectivity of DBT over different catalysts at a reaction temperature of 280 °C is shown in Table 5, which indicates

Table 5. Reaction Rate Constants and Selectivities of Different Catalysts

catalysts	S^a_{HYD} (%)	S^a_{DDS} (%)	HYD/DDS
b-MoS_2	23.67	76.33	0.31
H-NiMo-90−400	26.46	73.54	0.36
H-NiMo-120−400	26.93	74.07	0.35
H-NiMo-150−400	25.38	74.62	0.34
H-NiMo-180−400	26.93	74.07	0.35
H-NiMo-200−400	26.46	73.54	0.36
H-NiMo-150−350	23.31	76.69	0.32
H-NiMo-150−500	46.23	53.77	0.86
H-NiMo-150−600	52.82	47.18	1.12
N-NiMo-150−400	57.23	42.77	1.34

[a]Calculated at a reaction temperature of 280 °C.

that the HYD/DDS ratios of DBT are similar over catalysts prepared at different hydrothermal treatment temperatures. Interestingly, the HYD pathway selectivity of DBT on the catalysts increased with increasing calcination temperature in a H_2 atmosphere at the same hydrothermal treatment temperature and even the selectivity of the HYD pathway of DBT over that of the DDS pathway appeared in the H-NiMo-150−

https://doi.org/10.1021/acsomega.3c04059
ACS Omega 2023, 8, 41182−41193

600 catalyst samples. This result is due to the decomposition of part of the Ni−Mo−S structure into Ni_3S_2 when H-NiMo-150−500 and H-NiMo-150−600 are calcined in a H_2 atmosphere, which leads to an increase in the Ni_xS_y/Ni−Mo−S ratio. The mutual contact between Ni_xS_y and MoS_2 plates partially limits the accessibility of S vacancies in MoS_2 plates, making the DBT DDS reaction pathway limited.[65,86] Meanwhile, the hydrogen spillover phenomenon between Ni_xS_y and MoS_2 makes the catalyst more selective for the HYD pathway.[65] In contrast to other catalyst samples, DBT reacted with the highest HYD/DDS of 1.34 on the N-NiMo-150−400 sample prepared by calcination in a N_2 atmosphere. On the one hand, due to the limited amount of S activation of MoS_2 edge and corner sites in a N_2 atmosphere, which means that a very small amount of sulfur vacancies is generated, this is a prerequisite for DBT to carry out the DDS reaction pathway. On the other hand, the MoS_2 edge and corner active sites are covered by NiO obtained by decomposition, and under the reaction conditions, DBT acts as a vulcanizing agent to convert more NiO into Ni_xS_y (Figure 9), and the generation of Ni_xS_y facilitates the selectivity of the HYD pathway.

4. CONCLUSIONS

In summary, the hydrothermal treatment of commercial bulk MoS_2 and alkaline nickel carbonate, followed by calcination in either a H_2 or a N_2 atmosphere, yielded sulfided HDS catalysts with notable activity. The findings from characterization and HDS activity assessment indicated that the lateral size, number of stacked layers, and S/Mo atomic ratio of MoS_2 within the catalysts exhibited a decreasing trend, followed by an increasing trend as the hydrothermal treatment temperature increased. The optimal values for these parameters were achieved at a hydrothermal treatment temperature of 150 °C. Furthermore, the impact of various calcination temperatures on the catalyst structure was examined at the optimal hydrothermal treatment temperature. When subjected to a H_2 atmosphere, the MoS_2 plates underwent initial destruction and subsequent aggregation as the calcination temperature increased. Notably, the catalyst prepared at a calcination temperature of 400 °C exhibited the most favorable structure. Consequently, DBT demonstrated superior hydrodesulfurization (HDS) activity over H-NiMo-150−400. Additionally, it was further substantiated that the inclusion of Ni_xS_y contributed to an enhancement in the hydrogenation (HYD) selectivity of the catalysts, as evidenced by the HYD/DDS ratios of DBT in H-NiMo-150−500 and H-NiMo-150−600. This study not only enhances our comprehension of the formation mechanism of the Ni−Mo−S active phase in the HDS reaction and the impact of catalyst preparation conditions on its structure but also offers valuable insights for the advancement and implementation of novel, ecofriendly, and cost-effective catalysts for sulfide hydrogenation.

ASSOCIATED CONTENT

Supporting Information

The Supporting Information is available free of charge at https://pubs.acs.org/doi/10.1021/acsomega.3c04059.

Effects of hydrothermal treatment and H_2 atmosphere calcination on the structure of the catalyst: XRD analysis results, HRTEM analysis results, XPS analysis results and activity evaluation results of hydrothermal treatment only, calcination only and hydrothermal treatment before calcination; SEM-EDS and STEM-EDS analysis results of H-NiMo-150−400; Mo 3d spectra for different calcination conditions; and correlation between Ni−Mo−S content and activity (PDF)

AUTHOR INFORMATION

Corresponding Author

Qinghe Yang − *SINOPEC Research Institute of Petroleum Processing Co., Ltd., Beijing 100083, P. R. China*; Phone: +8610 82368123; Email: yangqh.ripp@sinopec.com; Fax: +8610 62311290

Authors

Chuangchuang Yang − *SINOPEC Research Institute of Petroleum Processing Co., Ltd., Beijing 100083, P. R. China*; orcid.org/0009-0004-9006-7512

Anpeng Hu − *SINOPEC Research Institute of Petroleum Processing Co., Ltd., Beijing 100083, P. R. China*

Qiaoling Dai − *SINOPEC Research Institute of Petroleum Processing Co., Ltd., Beijing 100083, P. R. China*

Ranran Hou − *SINOPEC Research Institute of Petroleum Processing Co., Ltd., Beijing 100083, P. R. China*

Zhiwei Liu − *SINOPEC Research Institute of Petroleum Processing Co., Ltd., Beijing 100083, P. R. China*; orcid.org/0000-0002-6566-1307

Complete contact information is available at: https://pubs.acs.org/10.1021/acsomega.3c04059

Notes

The authors declare no competing financial interest.

ACKNOWLEDGMENTS

The authorsare delighted to express our gratitude for the invaluable support extended to this research by the National Key Research and Development Project (Grant No. 2021YFA1501204) and the China Petrochemical Corporation (Sinopec Group 121043-2).

REFERENCES

(1) Gao, Y.; Han, W.; Long, X.; Nie, H.; Li, D. Preparation of hydrodesulfurization catalysts using MoS_3 nanoparticles as a precursor. *Appl. Catal., B* **2018**, *224*, 330−340.

(2) Wang, D.; Li, J.; Ma, H.; Yang, C.; Pan, Z.; Qu, W.; Tian, Z. Layer-structure adjustable MoS_2 catalysts for the slurry-phase hydrogenation of polycyclic aromatic hydrocarbons. *J. Energy Chem.* **2021**, *63*, 294−304.

(3) Guo, K.; Ding, Y.; Luo, J.; Yu, Z. Nickel Cobalt Thiospinel Nanoparticles as Hydrodesulfurization Catalysts: Importance of Cation Position, Structural Stability, and Sulfur Vacancy. *ACS Appl. Mater. Interfaces* **2018**, *10* (23), 19673−19681.

(4) Bodin, A.; Christoffersen, A. N.; Elkjaer, C. F.; Brorson, M.; Kibsgaard, J.; Helveg, S.; Chorkendorff, I. Engineering Ni−Mo-S Nanoparticles for Hydrodesulfurization. *Nano Lett.* **2018**, *18* (6), 3454−3460.

(5) Cao, H.; Bai, Z.; Li, Y.; Xiao, Z.; Zhang, X.; Li, G. Solvothermal Synthesis of Defect-Rich Mixed 1T-2H MoS_2 Nanoflowers for Enhanced Hydrodesulfurization. *ACS Sustainable Chem. Eng.* **2020**, *8* (19), 7343−7352.

(6) Zepeda, T. A.; de León, J. N. D.; Alonso, G.; Infantes-Molina, A.; Galindo-Ortega, Y. I.; Huirache-Acuña, R.; Fuentes, S. Hydrodesulfurization activity of Ni-containing unsupported Ga(x)WS_2 catalysts. *Catal. Commun.* **2019**, *130*, No. 105760.

(7) Yue, L.; Li, G.; Zhang, F.; Chen, L.; Li, X.; Huang, X. Size-dependent activity of unsupported Co−Mo sulfide catalysts for the

hydrodesulfurization of dibenzothiophene. *Appl. Catal., A* **2016**, *512*, 85−92.
(8) Bergwerff, J. A.; Visser, T.; Leliveld, G.; Rossenaar, B. D.; de Jong, K. P.; Weckhuysen, B. M. Envisaging the Physicochemical Processes during the Preparation of Supported Catalysts: Raman Microscopy on the Impregnation of Mo onto Al2O3 Extrudates. *J. Am. Chem. Soc.* **2004**, *126*, 14548−14556.
(9) Alsalme, A.; Alzaqri, N.; Alsaleh, A.; Siddiqui, M. R. H.; Alotaibi, A.; Kozhevnikova, E. F.; Kozhevnikov, I. V. Efficient Ni−Mo hydrodesulfurization catalyst prepared through Keggin polyoxometalate. *Appl. Catal., B* **2016**, *182*, 102−108.
(10) Füchtbauer, H. G.; Tuxen, A. K.; Li, Z.; Topsøe, H.; Lauritsen, J. V.; Besenbacher, F. Morphology and Atomic-Scale Structure of MoS_2 Nanoclusters Synthesized with Different Sulfiding Agents. *Top. Catal.* **2014**, *57* (1−4), 207−214.
(11) Walton, A. S.; Lauritsen, J. V.; Topsøe, H.; Besenbacher, F. MoS2 nanoparticle morphologies in hydrodesulfurization catalysis studied by scanning tunneling microscopy. *J. Catal.* **2013**, *308*, 306−318.
(12) Texier, S. Activation of alumina-supported hydrotreating catalysts by organosulfides: comparison with H_2S and effect of different solvents. *J. Catal.* **2004**, *223* (2), 404−418.
(13) Maity, S. K.; Ancheyta, J.; Soberanis, L.; Alonso, F.; Llanos, M. E. Alumina−titania binary mixed oxide used as support of catalysts for hydrotreating of Maya heavy crude. *Appl. Catal., A* **2003**, *244* (1), 141−153.
(14) Han, W.; Yuan, P.; Fan, Y.; Shi, G.; Liu, H.; Bai, D.; Bao, X. Preparation of supported hydrodesulfurization catalysts with enhanced performance using Mo-based inorganic−organic hybrid nanocrystals as a superior precursor. *J. Mater. Chem.* **2012**, *22* (48), 25340−25353.
(15) Wang, E.; Yang, F.; Song, M.; Chen, G.; Zhang, Q.; Wang, F.; Bing, L.; Wang, G.; Han, D. Recent advances in the unsupported catalysts for the hydrodesulfurization of fuel. *Fuel Process. Technol.* **2022**, *235*, No. 107386.
(16) Wang, G.; Chen, G.; Xie, W.; Wang, W.; Bing, L.; Zhang, Q.; Fu, H.; Wang, F.; Han, D. Three-dimensionally ordered macroporous bulk catalysts with enhanced catalytic performance for thiophene hydrodesulfurization. *Fuel Process. Technol.* **2020**, *199*, No. 106268.
(17) Liu, H.; Yin, C.; Li, X.; Chai, Y.; Li, Y.; Liu, C. Effect of NiMo phases on the hydrodesulfurization activities of dibenzothiophene. *Catal. Today* **2017**, *282*, 222−229.
(18) Chowdari, R. K.; de León, J. N. D.; Fuentes-Moyado, S. Template-free, facile synthesis of nickel promoted multi-walled MoS_2 & nano-bricks containing hierarchical MoS_2 nanotubes from the bulk NiMo oxide. *Appl. Catal., B* **2021**, *298*, No. 120617.
(19) Afanasiev, P. The influence of reducing and sulfiding conditions on the properties of unsupported MoS_2-based catalysts. *J. Catal.* **2010**, *269* (2), 269−280.
(20) Gao, Y.; Fang, X.; Cheng, Z.; Xu, L.; Lu, Z.; Wang, S. Exothermic effects and related surface properties of the ex situ presulfurized catalysts in fabrication and activation. *J. Ind. Eng. Chem.* **2015**, *26*, 202−209.
(21) Liu, B.; Liu, L.; Chai, Y.; Zhao, J.; Li, Y.; Liu, D.; Liu, Y.; Liu, C. Effect of sulfiding conditions on the hydrodesulfurization performance of the ex-situ presulfided CoMoS/γ-Al_2O_3 catalysts. *Fuel* **2018**, *234*, 1144−1153.
(22) Liu, B.; Liu, L.; Chai, Y.; Zhao, J.; Li, Y.; Liu, Y.; Liu, C. Highly Active CoMoS/Al_2O_3 Catalysts ex Situ Presulfided with Ammonium Sulfide for Selective Hydrodesulfurization of Fluid Catalytic Cracking Gasoline. *Ind. Eng. Chem. Res.* **2018**, *57* (6), 2041−2049.
(23) Mahmoudabadi, Z. S.; Rashidi, A.; Tavasoli, A.; Esrafili, M.; Panahi, M.; Askarieh, M.; Khodabakhshi, S. Ultrasonication-assisted synthesis of 2D porous MoS_2/GO nanocomposite catalysts as high-performance hydrodesulfurization catalysts of vacuum gasoil: Experimental and DFT study. *Ultrason. Sonochem.* **2021**, *74*, No. 105558.
(24) Muscuso, L.; Cravanzola, S.; Cesano, F.; Scarano, D.; Zecchina, A. Optical, Vibrational, and Structural Properties of MoS_2 Nanoparticles Obtained by Exfoliation and Fragmentation via Ultrasound Cavitation in Isopropyl Alcohol. *J. Phs. Chem. C* **2015**, *119* (7), 3791−3801.
(25) Tumen-Ulzii, N.; Batnasan, A.; Gunchin, B. Selective dissolution of copper and iron from molybdenite concentrate using acidic sodium nitrate solution. *Miner. Eng.* **2022**, *185*, No. 107715.
(26) Hojamberdiev, M.; Goel, N.; Kumar, R.; Kadirova, Z. C.; Kumar, M. Efficient NO_2 sensing performance of a low-cost nanostructured sensor derived from molybdenite concentrate. *Green Chem.* **2020**, *22* (20), 6981−6991.
(27) Daage, M.; Chianelli, R. R. Structure-Function Relations in Molybdenum Sulfide Catalysts: The "Rim-Edge" Model. *J. Catal.* **1994**, 414−427.
(28) Hu, K. H.; Hu, X. G.; Sun, X. J. Morphological effect of MoS_2 nanoparticles on catalytic oxidation and vacuum lubrication. *Appl. Surf. Sci.* **2010**, *256* (8), 2517−2523.
(29) Yi, Y.; Jin, X.; Wang, L.; Zhang, Q.; Xiong, G.; Liang, C. Preparation of unsupported Ni−Mo−S catalysts for hydrodesulfurization of dibenzothiophene by thermal decomposition of tetramethylammonium thiomolybdates. *Catal. Today* **2011**, *175* (1), 460−466.
(30) Lumbreras, J. A.; Huirache-Acuña, R.; Rivera-Muñoz, E. M.; Berhault, G.; Alonso-Núñez, G. Unsupported Ni/Mo(W)S_2 Catalysts from Hexamethylenediammonium Thiometallates Precursors: In Situ Activation During the HDS of DBT. *Catal. Lett.* **2010**, *134* (1−2), 138−146.
(31) Wang, Z.-j.; Wu, P.; Lan, L.; Liu, K.; Hu, Y.; Ji, S. Preparation, characterization and hydrodesulfurization performances of Co-Ni_2P/SBA-15 catalysts. *J. Energy Chem.* **2015**, *24* (2), 185−192.
(32) Yoosuk, B.; Kim, J. H.; Song, C.; Ngamcharussrivichai, C.; Prasassarakich, P. Highly active MoS_2, $CoMoS_2$ and $NiMoS_2$ unsupported catalysts prepared by hydrothermal synthesis for hydrodesulfurization of 4,6-dimethyldibenzothiophene. *Catal. Today* **2008**, *130* (1), 14−23.
(33) Ye, L.; Xu, H.; Zhang, D.; Chen, S. Synthesis of bilayer MoS_2 nanosheets by a facile hydrothermal method and their methyl orange adsorption capacity. *Mater. Res. Bull.* **2014**, *55*, 221−228.
(34) Liu, Y. D.; Ren, L.; Qi, X.; Yang, L. W.; Hao, G. L.; Li, J.; Wei, X. L.; Zhong, J. X. Preparation, characterization and photoelectrochemical property of ultrathin MoS_2 nanosheets via hydrothermal intercalation and exfoliation route. *J. Alloys Compd.* **2013**, *571*, 37−42.
(35) Wang, T.; Zhang, X.; Mei, L.; Ma, D.; Liao, Y.; Zu, Y.; Xu, P.; Yin, W.; Gu, Z. A two-step gas/liquid strategy for the production of N-doped defect-rich transition metal dichalcogenide nanosheets and their antibacterial applications. *Nanoscale* **2020**, *12* (15), 8415−8424.
(36) Rajendhran, N.; Palanisamy, S.; Periyasamy, P.; Venkatachalam, R. Enhancing of the tribological characteristics of the lubricant oils using Ni-promoted MoS_2 nanosheets as nano-additives. *Tribol. Int.* **2018**, *118*, 314−328.
(37) Backes, C.; Berner, N. C.; Chen, X.; Lafargue, P.; LaPlace, P.; Freeley, M.; Duesberg, G. S.; Coleman, J. N.; McDonald, A. R. Functionalization of liquid-exfoliated two-dimensional 2H-MoS_2. *Angew. Chem., Int. Ed.* **2015**, *54* (9), 2638−2642.
(38) Rajendhran, N.; Palanisamy, S.; Periyasamy, P.; Venkatachalam, R. Enhancing of the tribological characteristics of the lubricant oils using Ni-promoted MoS_2 nanosheets as nano-additives. *Tribol. Int.* **2018**, *118* (114), 314−328.
(39) Chao, Y.; Ge, Y.; Chen, Z.; Cui, X.; Zhao, C.; Wang, C.; Wallace, G. G. One-Pot Hydrothermal Synthesis of Solution-Processable MoS2/PEDOT:PSS Composites for High-Performance Supercapacitors. *ACS Appl. Mater. Interfaces* **2021**, *13* (6), 7285−7296.
(40) Wang, Q.; Li, X.; Ma, X.; Li, Z.; Yang, Y. Activation of the MoS_2 Basal Plane to Enhance CO Hydrogenation to Methane Activity Through Increasing S Vacancies. *ACS Appl. Mater. Interfaces* **2022**, *14* (6), 7741−7755.
(41) Sun, K.; Guo, H.; Jiao, F.; Chai, Y.; Li, Y.; Liu, B.; Mintova, S.; Liu, C. Design of an intercalated Nano-MoS_2 hydrophobic catalyst

https://doi.org/10.1021/acsomega.3c04059
ACS Omega 2023, 8, 41182−41193

with high rim sites to improve the hydrogenation selectivity in hydrodesulfurization reaction. *Appl. Catal., B* **2021**, *286*, No. 119907.
(42) Liu, S.; Zhang, X.; Zhang, J.; Lei, Z.; Liang, X.; Chen, B. MoS_2 with tunable surface structure directed by thiophene adsorption toward HDS and HER. *Sci. China Mater.* **2016**, *59* (12), 1051−1061.
(43) Wang, S.; Tu, J.; Xiao, J.; Zhu, J.; Jiao, S. 3D skeleton nanostructured Ni_3S_2/Ni foam@RGO composite anode for high-performance dual-ion battery. *J. Energy Chem.* **2019**, *28*, 144−150.
(44) Wu, B.; Qian, H.; Nie, Z.; Luo, Z.; Wu, Z.; Liu, P.; He, H.; Wu, J.; Chen, S.; Zhang, F. Ni_3S_2 nanorods growing directly on Ni foam for all-solid-state asymmetric supercapacitor and efficient overall water splitting. *J. Energy Chem.* **2020**, *46*, 178−186.
(45) Han, D.; Li, Q.; Wang, E.; Xie, W.; Chen, G.; Zhang, Q.; Bing, L.; Wang, F.; Fu, H.; Wang, G. The evolution of NiMo unsupported catalysts with 3DOM structure for thiophene hydrodesulfurization. *Catal. Today* **2022**, *405*−*406*, 329−336.
(46) Li, S.; Liu, Y.; Zhao, X.; Cui, K.; Shen, Q.; Li, P.; Qu, X.; Jiao, L. Molecular Engineering on MoS_2 Enables Large Interlayers and Unlocked Basal Planes for High-Performance Aqueous Zn-Ion Storage. *Angew. Chem., Int. Ed.* **2021**, *60* (37), 20286−20293.
(47) Lai, W.; Chen, Z.; Zhu, J.; Yang, L.; Zheng, J.; Yi, X.; Fang, W. A NiMoS flower-like structure with self-assembled nanosheets as high-performance hydrodesulfurization catalysts. *Nanoscale* **2016**, *8* (6), 3823−3833.
(48) Wang, S.; An, C.; Yuan, J. Synthetic Fabrication of Nanoscale MoS_2-Based Transition Metal Sulfides. *Materials* **2010**, *3* (1), 401−433.
(49) Lian, T.; Li, X.; Wang, Y.; Zhu, S.; Yang, X.; Liu, Z.; Ye, C.; Liu, J.; Li, Y.; Su, B.; Chen, L. Boosting Highly Active Exposed Mo Atoms by Fine-Tuning S-Vacancies of MoS_2-Based Materials for Efficient Hydrogen Evolution. *ACS Appl. Mater. Interfaces* **2022**, *14* (27), 30746−30759.
(50) Li, X.; Guo, Y.; Yan, L.; Yan, T.; Song, W.; Feng, R.; Zhao, Y. Enhanced activation of peroxymonosulfate by ball-milled MoS_2 for degradation of tetracycline: Boosting molybdenum activity by sulfur vacancies. *Chem. Eng. J.* **2022**, *429*, No. 132234, DOI: 10.1016/j.cej.2021.132234.
(51) Li, L.; Qin, Z.; Ries, L.; Hong, S.; Michel, T.; Yang, J.; Salameh, C.; Bechelany, M.; Miele, P.; Kaplan, D.; et al. Role of Sulfur Vacancies and Undercoordinated Mo Regions in MoS_2 Nanosheets toward the Evolution of Hydrogen. *ACS Nano* **2019**, *13* (6), 6824−6834.
(52) Venkateshwaran, S.; Josline, M. J.; Kumar, S. M. S. Fine-tuning interlayer spacing in MoS_2 for enriching 1T phase via alkylated ammonium ions for electrocatalytic hydrogen evolution reaction. *Int. J. Hydrogen Energy* **2021**, *46* (12), 8377−8390.
(53) Nguyen-Ba, K.; Vargas-García, J. R.; Manzo-Robledo, A. Alternative synthesis of structurally defective MoS_2 nanoflakes for efficient hydrogen evolution reaction. *Mater. Sci. Eng.: B* **2020**, *256*, No. 114539.
(54) Han, W.; Nie, H.; Long, X.; Li, M.; Yang, Q.; Li, D. A study on the origin of the active sites of HDN catalysts using alumina-supported MoS_3 nanoparticles as a precursor. *Catal. Sci. Technol.* **2016**, *6* (10), 3497−3509.
(55) Fan, R.; Zhou, J.; Xun, W.; Cheng, S.; Vanka, S.; Cai, T.; Ju, S.; Mi, Z.; Shen, M. Highly efficient and stable Si photocathode with hierarchical MoS_2/Ni_3S_2 catalyst for solar hydrogen production in alkaline media. *Nano Energy* **2020**, *71*, No. 104631.
(56) Lei, Y.; Li, W.; Xiao, X.; Zhang, H.; Ma, T.; Ma, C. One-step construction of cubic-like NiS_2@MoS_2 nanocrystals for improved electrocatalytic performance. *J. Mater. Sci.: Mater. Electron.* **2022**, *33* (14), 11154−11164.
(57) Nguyen, D. C.; Doan, T. L. L.; Prabhakaran, S.; Tran, D. T.; Kim, D. H.; Lee, J. H.; Kim, N. H. Hierarchical Co and Nb dual-doped MoS_2 nanosheets shelled micro-TiO_2 hollow spheres as effective multifunctional electrocatalysts for HER, OER, and ORR. *Nano Energy* **2021**, *82*, No. 105750, DOI: 10.1016/j.nanoen.2021.105750.
(58) Zhang, S.; Liu, X.; Liu, C.; Luo, S.; Wang, L.; Cai, T.; Zeng, Y.; Yuan, J.; Dong, W.; Pei, Y.; Liu, Y. MoS_2 Quantum Dot Growth Induced by S Vacancies in a ZnIn2S4Monolayer: Atomic-Level Heterostructure for Photocatalytic Hydrogen Production. *ACS Nano* **2018**, *12* (1), 751−758.
(59) Ramos, M.; Berhault, G.; Ferrer, D. A.; Torres, B.; Chianelli, R. R. HRTEM and molecular modeling of the MoS_2−Co_9S_8interface: understanding the promotion effect in bulk HDS catalysts. *Catal. Sci. Technol.* **2012**, *2* (1), 164−178.
(60) Lauritsen, J. V.; Bollinger, M. V.; Lægsgaard, E.; Jacobsen, K. W.; Nørskov, J. K.; Clausen, B. S.; Topsøe, H.; Besenbacher, F. Atomic-scale insight into structure and morphology changes of MoS_2 nanoclusters in hydrotreating catalysts. *J. Catal.* **2004**, *221* (2), 510−522.
(61) Liu, Z.; Han, W.; Hu, D.; Sun, S.; Hu, A.; Wang, Z.; Jia, Y.; Zhao, X.; Yang, Q. Effects of Ni−Al_2O_3 interaction on NiMo/Al_2O_3 hydrodesulfurization catalysts. *J. Catal.* **2020**, *387*, 62−72.
(62) Eijsbouts, S.; Anderson, G. H.; Bergwerff, J. A.; Jacobi, S. Economic and technical impacts of replacing Co and Ni promotion in hydrotreating catalysts. *Appl. Catal., A* **2013**, *458*, 169−182.
(63) Eijsbouts, S.; Li, X.; Bergwerff, J.; Louwen, J.; Woning, L.; Loos, J. Nickel sulfide crystals in Ni−Mo and Ni-W catalysts: Eye-catching inactive feature or an active phase in its own right? *Catal. Today* **2017**, *292*, 38−50.
(64) Kuriki, Y.; Yumura, M.; Ohshima, S.; Uchida, K.; Ikazaki, F.Synthesis and Catalytic Activity of Ultra Fine Metal Sulfide Particles. In *Coal Science, Proceedings of the Eighth International Conference on Coal Science*; Elsevier, 1995; Vol. *24*, pp 1347−1350.
(65) Vogelgsang, F.; Ji, Y.; Shi, H.; Lercher, J. A. On the multifaceted roles of NiSx in hydrodearomatization reactions catalyzed by unsupported Ni-promoted MoS_2. *J. Catal.* **2020**, *391*, 212−223.
(66) Baeza, P.; Villarroel, M.; Ávila, P.; Agudo, A. L.; Delmon, B.; Gil-Llambías, F. J. Spillover hydrogen mobility during Co−Mo catalyzed HDS in industrial-like conditions. *Appl. Catal., A* **2006**, *304*, 109−115.
(67) Karroua, M.; Matralis, H.; Grange, P.; Delmon, B. Unsupported NiMo Catalysts. Influence of the Sulfinding Temperature and Evolution of the Unsupported NiMoS Phase during Reaction. *Bull. Soc. Chim. Belg.* **2010**, *104*, 11−18.
(68) Villarroel, M.; Camú, E.; Escalona, N.; Ávila, P.; Rasmussen, S. B.; Baeza, P.; Gil-Llambías, F. Synergisms via hydrogen spillover between some transition metals during hydrodesulphurization: Increased activity towards conversion of refractory molecules. *Appl. Catal., A* **2011**, *399* (1−2), 63−68.
(69) Karroua, M.; Matralis, M.; Grange, P.; Delmon, B. Unsupported NiMo Catalysts. Influence of the Sulfinding Temperature and Evolution of the Unsupported NiMoS Phase during Reaction. *Bull. Soc. Chim. Belg.* **2010**, *104* (1), 11−18.
(70) de Brimont, M. R.; Dupont, C.; Daudin, A.; Geantet, C.; Raybaud, P. Deoxygenation mechanisms on Ni-promoted MoS_2 bulk catalysts: A combined experimental and theoretical study. *J. Catal.* **2012**, *286*, 153−164.
(71) Eijsbouts, S. On the flexibility of the active phase in hydrotreating catalysts. *Appl. Catal., A* **1997**, *158* (1−2), 53−92.
(72) He, K. L.; Liu, N.; Zheng, R. Y.; Liu, W. Y.; Li, B.; Wang, Z. Y. Synthesis and Characterization of SiC Nanoparticles with Lamellar Structures from Taixi Coal. *Adv. Mater. Res.* **2013**, *785*−*786*, 488−492.
(73) Henmi, H.; Mori, M.; Hirayama, T.; et al. Influence of the self-generated and controlled atmosphere on the thermal decomposition of basic nickel carbonate, $NiCO_3 \cdot 2Ni(OH)_2 \cdot 4H_2O$. *Thermochim. Acta* **1986**, *104*, 101−109.
(74) Hu, J.; Yu, L.; Deng, J.; Wang, Y.; Cheng, K.; Ma, C.; Zhang, Q.; Wen, W.; Yu, S.; Pan, Y.; et al. Sulfur vacancy-rich MoS_2 as a catalyst for the hydrogenation of CO_2 to methanol. *Nat. Catal.* **2021**, *4* (3), 242−250.
(75) Lauritsen, J.; Kibsgaard, J.; Olesen, G.; Moses, P.; Hinnemann, B.; Helveg, S.; Norskov, J.; Clausen, B.; Topsoe, H.; Lagsgaard, E. Location and coordination of promoter atoms in Co- and Ni-

promoted MoS_2-based hydrotreating catalysts. *J. Catal.* **2007**, *249* (2), 220−233.
(76) Besenbacher, F.; Brorson, M.; Clausen, B. S.; Helveg, S.; Hinnemann, B.; Kibsgaard, J.; Lauritsen, J. V.; Moses, P. G.; Nørskov, J. K.; Topsøe, H. Recent STM, DFT and HAADF-STEM studies of sulfide-based hydrotreating catalysts: Insight into mechanistic, structural and particle size effects. *Catal. Today* **2008**, *130* (1), 86−96.
(77) Wu, P. R.; Liu, Z.; Cheng, Z. L. Hydrothermal-assisted shearing exfoliation for few-layered MoS_2 nanosheets. *RSC Adv.* **2019**, *9* (30), 17016−17024.
(78) Yin, C.; Wang, Y.; Xue, S.; Liu, H.; Li, H.; Liu, C. Influence of sulfidation conditions on morphology and hydrotreating performance of unsupported Ni−Mo−W catalysts. *Fuel* **2016**, *175*, 13−19.
(79) Liu, H.; Liu, Q.; Zhang, J.; Yin, C.; Zhao, Y.; Yin, S.; Liu, C.; Sun, W. PVP-assisted synthesis of unsupported NiMo catalysts with enhanced hydrodesulfurization activity. *Fuel Process. Technol.* **2017**, *160*, 93−101.
(80) Han, W.; Nie, H.; Long, X.; Li, D. A study on the role of Ni atoms in the HDN activity of $NiMoS_2/Al_2O_3$ catalyst. *Appl. Catal., A* **2020**, *593*, No. 117458.
(81) Zhang, L.-F.; Ke, X.; Ou, G.; Wei, H.; Wang, L.-N.; Wu, H. Defective MoS_2 electrocatalyst for highly efficient hydrogen evolution through a simple ball-milling method. *Sci. China Mater.* **2017**, *60* (9), 849−856.
(82) Li, J.; Kang, J.; Cai, Q.; Hong, W.; Jian, C.; Liu, W.; Banerjee, K. Boosting Hydrogen Evolution Performance of MoS_2 by Band Structure Engineering. *Adv. Mater. Interfaces* **2017**, *4* (16), No. 1700303, DOI: 10.1002/admi.201700303.
(83) Rhamdhani, M. A.; Jak, E.; Hayes, P. C. Basic Nickel Carbonate: Part I. Microstructure and Phase Changes during Oxidation and Reduction Processes. *Metall. Mater. Trans. B* **2008**, *39* (2), 218−233.
(84) Rhamdhani, M. A.; Jak, E.; Hayes, P. C. Basic Nickel Carbonate: Part II. Microstructure Evolution during Industrial Nickel Production from Basic Nickel Carbonate. *Metall. Mater. Trans. B* **2008**, *39* (2), 234−245.
(85) Altamirano, E.; Delosreyes, J.; Murrieta, F.; Vrinat, M. Hydrodesulfurization of dibenzothiophene and 4,6-dimethyl-dibenzothiophene: Gallium effect over NiMo/AlO sulfided catalysts. *J. Catal.* **2005**, *235* (2), 403−412.
(86) Wagenhofer, M. F.; Shi, H.; Gutiérrez, O. Y.; Jentys, A.; Lercher, J. A. Enhancing hydrogenation activity of Ni−Mo sulfide hydrodesulfurization catalysts. *Sci. Adv.* **2020**, *6* (19), No. eaax5331.

https://doi.org/10.1021/acsomega.3c04059
ACS Omega 2023, 8, 41182−41193